Earth, Planets and Space

FULL PAPER Open Access

Permutation entropy variations in seismic noise before and after eruptive activity at Shinmoedake volcano, Kirishima complex, Japan

K. I. Konstantinou[1*], D. A. Rahmalia[1], I. Nurfitriana[1,2] and M. Ichihara[3]

Abstract

Permutation entropy (PE) is a complexity metric that encodes a time series into sequences of symbols and can be used to decipher between deterministic and stochastic behavior. This study investigates PE variations in seismic noise during three eruption cycles in 2011, 2017, and 2018 at Shinmoedake volcano, Japan. The volcano is monitored by a dedicated seismic network and by infrasound microphones that recorded continuously during the aforementioned eruptions. The frequency range 1–7 Hz was used in order to infer temporal changes of PE in seismic noise and minimize any human contributions. The results showed that PE values decreased before the occurrence of each eruption. By combining these results with other observations we can attribute this decrease in PE to two reasons: first, to the occurrence of volcanic tremor that is a deterministic signal, and second, to magma migration at shallower depth beneath Shinmoedake which can attenuate high-frequency seismic waves and thus result in a less stochastic signal. PE also exhibited a spike-like increase just before the onset of the three eruptions. In 2011 and 2017, this feature was probably associated with bubble growth and collapse due to the interaction between the aquifer and high temperature magma. In 2018 the aquifer had mostly evaporated; hence, the spike in PE values was likely generated by fracturing of solidified magma within the conduit as fresh magma was pushing its way upwards. These results show that PE is a potentially useful tool for monitoring seismic noise at volcanoes and can contribute toward forecasting volcanic eruptions in conjunction with other widely used methodologies.

Keywords: Permutation Entropy, Shinmoedake, Japan, Volcanic tremor, Eruption, Seismic noise

*Correspondence: kkonst@cc.ncu.edu.tw

[1] Department of Earth Sciences, National Central University, Jhongli 320, Taiwan
Full list of author information is available at the end of the article

Graphical Abstract

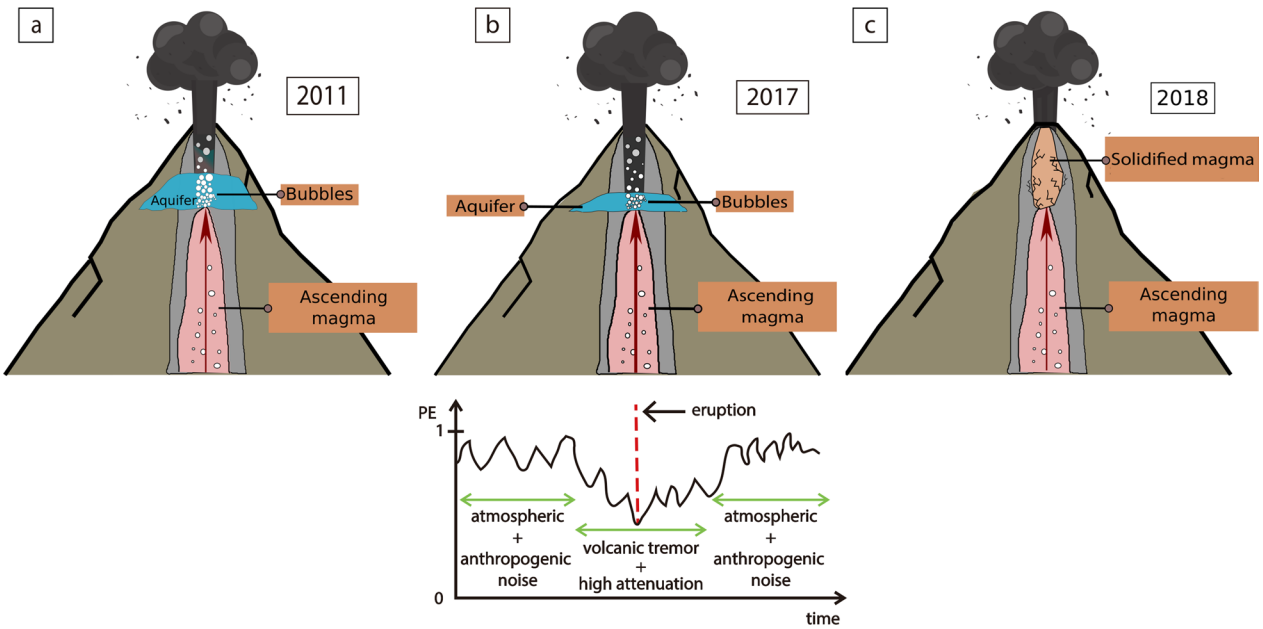

Introduction

Volcanism in southern Kyushu, Japan, is the result of the subduction of the southern segment of the Philippine Sea plate beneath the Eurasian plate (Kamata and Kodama 1999). The Kagoshima graben is a trough-shaped volcano-tectonic depression in the southern part of Kyushu island, which trends in NNE–SSW direction with a dimension of 120×30 km and contains the Kirishima volcano complex (Kamata and Kodama 1999; Maeno and Taniguchi 2007) (Fig. 1). Kirishima is a basaltic-andesite volcano group that has been active in the past 22 ka as manifested by intense volcanic and geothermal activity (Imura 1992; Kagiyama 1994; Kato and Yamasato 2013). Shinmoedake volcano is one of the most active volcanoes of this group and is located in the center of the Kirishima complex (Kato and Yamasato 2013; Nakao et al. 2013). A new eruptive cycle at Shinmoedake resumed on 22 August 2008 after a long quiescent period since 1716–1717 CE when its last magmatic eruption occurred. The new cycle started with a small-scale phreatic eruption on 19 January 2011 which formed a fissure 800 m long aligned along the E–W direction (Imura 1992; Geshi et al. 2010). The first magmatic eruption of the sequence occurred on 26 January 2011 and continued until 27 January 2011 (Nakada et al. 2013). This phreatomagmatic eruption was followed by volcanic tremor whose source was located beneath the main crater, indicating that it was likely the result of magma movement (Ichihara and Matsumoto 2017). The 2011 eruption consisted of subplinian events, lava effusion, and vulcanian explosions. Prior to the 2011 eruption, the Japan Meteorological Agency (JMA) reported that deformation was observed from the end of 2009 until January 2011 and was also accompanied by increased seismicity from October 2010. The deformation recorded NW of Shinmoedake crater was subsequently interpreted as accumulation of melt in the magma chamber prior to the 2011 eruption (Kato and Yamasato 2013; Nakao et al. 2013).

After a second quiescent period lasting 6 years Shinmoedake erupted again on 11 October 2017. Ash emissions continued until 17 October and were accompanied by volcanic tremor until 21 October. The 2017 eruption was preceded by low-frequency (LF) events and deformation of the volcano edifice 38 h before the onset of ash emission (Yamada et al. 2019). LF events and changes in the tilt record indicated increased fluid activity, such as magma intrusion (Yamada et al. 2019). Volcanic seismicity was still taking place at relatively high levels until March 2018. Another eruption occurred from 1 to 9 March 2018 producing 47 explosions that consisted of ash emission followed by lava emplacement. The last stage of the 2018 eruption occurred from 10 March until 27 June 2018 and was characterized by intermittent vulcanian eruptions. Prior to the 2018 eruption there was no clear precursor observed either in terms of deformation or increased seismicity. A slight tilt change was recorded

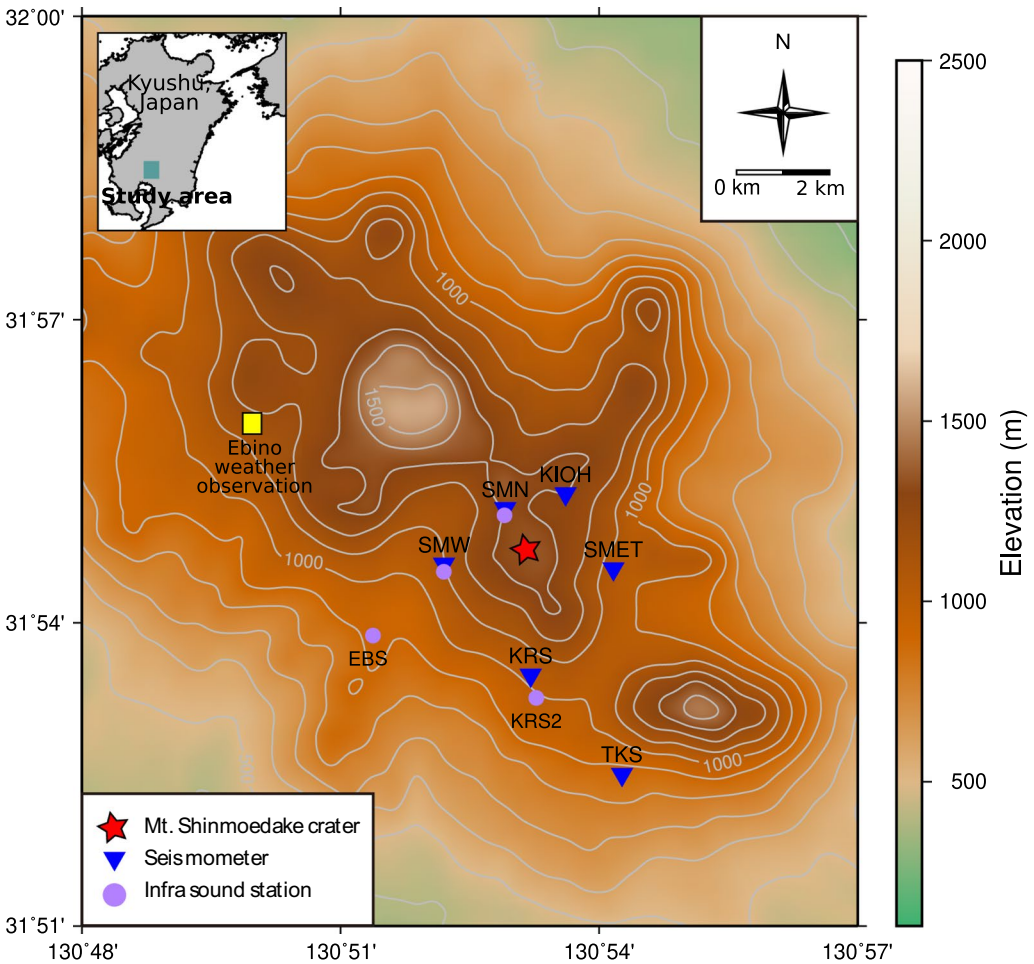

Fig. 1 Topographic map of Shinmoedake volcano also showing the locations of seismic, infrasound, and weather stations in the area that are used in this study. The small inset in the upper left corner displays a map of Kyushu island and the location of the Kirishima complex as a solid square

at some stations; however, it was not clearly related to the volcanic activity. In addition, no significant high-frequency (HF) or LF earthquake activity was associated with the onset of ash emission in 2018 (Yamada et al. 2019). LF events and volcanic tremor gradually increased after 1 March and the deformation changed to contraction during the lava extrusion phase.

Seismic noise cross-correlation has long been utilized as a tool for monitoring velocity changes at active volcanoes both in terms of spatial and temporal variations (e.g., Brenguier et al. 2008; Obermann et al. 2011). This methodology was applied to seismic noise recorded at Shinmoedake; however, the results revealed only minor changes in seismic velocity prior to the 2011 eruption and very little change before the 2017–2018 eruptions (Nishida et al. 2020). In this work we use seismic noise in order to calculate Permutation Entropy (hereafter referred to as PE) and reconstruct its temporal variation prior to and during the three eruption cycles at Shinmoedake. PE is a metric that quantifies the degree of randomness in a time series and its application to other volcanoes previously (see Glynn and Konstantinou 2016; Melchor et al. 2020) has shown promise in recognizing precursory changes prior to eruptions. First, we begin with a description of the seismic network around Shinmoedake, the data availability, and with a general introduction to the methodology we used. Results for each eruptive cycle are then presented and correlated with other geophysical or geodetic observations. In the last part of this work, we investigate the statistical significance of PE variations and we discuss our results in the framework of physical processes during the eruptions as well as their importance for volcano monitoring.

Data

The Earthquake Research Institute of the University of Tokyo (ERI) has deployed a permanent seismic network at the Kirishima volcano group which consists of 10 stations and is also affiliated with JMA, the National Research Institute for Earth Science and Disaster Resilience (NIED), as well as the Institute of Seismology and Volcanology of Kyushu University. This study utilized the seismic data that was recorded during January 2011, 23 September–31 October 2017 (hereafter September–October 2017), and 6 February–31 March 2018 (hereafter February–March 2018) based on the eruption sequences. We used 6 stations (SMN, SMW, KIOH, SMET, KRS, TKS) that were equipped with three-component sensors and recorded with a sampling rate of 100 Hz. These stations had a high signal-to-noise ratio and exhibited good azimuthal coverage around Shinmoedake volcano (Fig. 1). In general, all the stations were located less than 3 km from Shinmoedake crater, except TKS. SMN, SMW, and TKS are equipped with Nanometrics Trillium-120 broadband seismometers. The rest of the stations are equipped with short-period seismometers having a flat frequency response starting from 1 Hz. In addition to the seismic stations, a Hakusan SI102 infrasound microphone was installed at station SMN in January 2011. After the 2011 subplinian eruption, an infrasound microphone was also installed at stations SMW, KRS2, and EBS. Stations KIOH and SMN were damaged by the 2011 eruption and the seismometer had to be re-installed at SMN in June 2012.

Permutation entropy variation

Methodology

Permutation entropy quantifies information based on the existence of permutation patterns in a time series by combining the concept of entropy and symbolic dynamics (Bandt and Pompe 2002; Riedl et al. 2013). In order to calculate PE the samples of the time series $x(i)$ are first embedded into delay vectors of the form $x(i)$, $x(i+L)$,... ,$x(i+(m\text{-}1))L$, where i is the sample index, L is the delay (multiple of the sampling interval), and m is the Euclidean dimension. The elements of the delay vectors are then assigned a rank number starting from the smallest value which has a rank equal to 1 (e.g., the delay vector {3, 1, 4} has rank sequence 2,1,3) and then this sequence of ranks represents a distinct symbol. In this way any time series can be partitioned into a sequence of symbols so that for *m!* distinct symbols the Shannon entropy is defined as

$$H_p(m) = -\sum_{j=1}^{m!} P_j \ln P_j, \quad (1)$$

where the probability distribution of each distinct symbol (with $j = 1, 2, 3, \ldots, m!$) is represented as P_j. Usually $H_p(m)$ is divided by $\ln(m!)$; hence, PE will assume values that will vary within the interval 0–1 with PE equal to 0 signifying periodic signals and PE equal to 1 corresponding to fully stochastic ones. The selection of optimal L and m as well as time window length W (in number of samples) is essential to distinguish between stochastic and deterministic signals. Small values of $m = 1$ or 2 may not recognize dynamical changes optimally, while the selection of large values of m, such as 12 or 15, requires significant computational time (Cao et al. 2004; Staniek and Lehnertz 2007). We calculate PE for the vertical component of stations SMN, SMW, KIOH, KRS, and TKS after bandpass filtering the continuous waveforms between 1 and 7 Hz. This band corresponds mostly to volcanic activity and minimizes contributions from other sources, such as meteorological conditions or anthropogenic noise (Nishida et al. 2020).

Bandt and Pompe (2002) recommended that $m = 3,\ldots,7$, $L = 1$ and $W > > m!$ for practical applications, while Cao et al. (2004) concluded that the most appropriate values of m are 5, 6, or 7. The PE application on field experiments was also analyzed by Riedl et al. (2013) using different types of time series in order to choose the optimal embedding parameters. Results showed that time series related to dynamical processes, such as heart rate signals commonly used $L = 1$, $m = 7$. Amigó et al. (2008) suggested that W should be larger than 5 $m!$ in order to include all possible patterns within a particular time series and to distinguish easily between deterministic and random behavior. We tested different values of m, L, in order to determine their optimal values by calculating PE for $m = 5$, 6 and $L = 1$, 2, 3, 4, 5 during October 2017 (Additional file 1: Fig. S1–S5). According to these tests, varying m did not change PE values significantly, while varying L produced increasing PE values; however, this caused no significant change in the PE temporal pattern. We chose $m = 5$ and $L = 2$ based on considerations regarding the computational time needed and the variation that these values exhibit compared to other values. For $m = 5$ and $L = 2$, the window length W had to be larger than 5 $m!$ (i.e., 600 data samples); hence, in this study we used 20 min as our window length, which is equal to $W = 120{,}000$ data samples. We also estimated spectrograms for each station by using the short-time Fourier Transform and by applying a moving window of 20 s with 50% overlap, plotting the spectrograms alongside the PE temporal variation. We chose this way of presenting our results for the reason that PE depends on the number of frequencies present in the time series (see, for example, Cao et al. 2004); hence, PE and the frequency evolution should be viewed jointly. However, we also include Additional file 1: Figs. S6–S8 in the supporting

information that display only the PE variation for each of the three eruptive periods under study.

Results

PE variations during the eruption cycles in January 2011, September–October 2017, and February–March 2018, can be divided into 3 periods based on their general characteristics. During period I, PE variation was characterized by periodically increasing and decreasing values in a timescale from hours to days. During period II, PE started to decrease up to the onset of the eruption and tended to have lower values compared to the other periods. The period after the onset of the eruption was defined as period III. SMN and SMW are the closest stations to the eruption site and are located around 0.8 and 1.2 km from the Shinmoedake crater, respectively. These stations showed similar PE variations that ranged from 0.5 to 0.9 (Figs. 2 and 3). Period I in these stations extended from 1 to 17 January 2011, from 23 September to 9 October 2017, and between 6 and 22 February 2018. Period I during September–October 2017 and February–March 2018 did not exhibit any regular patterns. Period II during the three eruption cycles had different duration. The decreasing PE values during period II occurred 7 and 2 days before the eruption in January 2011 and September–October 2017, respectively. PE decreased from around 0.73 to 0.68 at SMN and from 0.72 to 0.65 at SMW, while these decreases also coincided with the onset/occurrence of eruption tremor. It should be noted that the decrease in PE is not clear before the 2018 eruption either at SMN or SMW. We also observed an interesting feature in the form of PE increasing and then suddenly dropping, similar to a spike, just before the onset of the eruptions. This feature can be seen at SMN a few hours prior to the small phreatic eruption on 19 January 2011 and again before the magmatic eruption on 26 January (cf. Fig. 2). The same spike-like feature can be clearly observed again at SMN and SMW prior to the onset of the 2017 and 2018 eruptions. After the onset of the eruption (period III), PE exhibited similar behavior at SMN and SMW stations during the three eruption cycles. Lower PE values were observed for several days after the eruptions in 2017 and 2018 (coinciding again with eruption tremor) and then they were followed by progressively increasing PE values.

The other stations, such as KIOH, SMET and KRS, which were located about 2 km from the Shinmoedake crater, captured similar PE behavior (Figs. 4 and 5). These stations observed each period (period I, period II, period III) clearly with no data gaps. PE variation at station KIOH resembles that of SMN and SMW with values that range from 0.5 to 0.8 and a significant drop several days prior to the 2011 eruption. A small spike can also be seen at KIOH just before the onset of the 2011 eruptions, while PE values start increasing a few days afterward. Station SMET shows a gradual decrease in PE values from about 0.85 to 0.7 prior to the 2017 eruption and then a further decrease that coincides with the occurrence of eruption tremor until 22 October when tremor activity weakens. During the eruption cycle in 2018 station SMET exhibits again similar behavior with stations SMN and SMW, in the sense that there is a spike in PE variation just before the onset of the eruption. Lower PE values also appear to coincide with the onset of eruption tremor, while PE increased significantly after tremor had ceased. The situation at station KRS is the same as described previously for SMN and SMW with the difference that there is a significant daily variation of PE values after the 2018 eruption starting on 11 March until the end of the observation period. Finally, station TKS did not exhibit PE behavior similar to any of the aforementioned stations and the different periods cannot be identified clearly (Additional file 1: Fig. S9). This is probably due to the fact that TKS is located about 4.6 km away from the Shinmoedake crater.

In order to investigate whether the changes in PE variation between the different periods are statistically significant, we performed a Kolmogorov–Smirnov test. The null hypothesis of this test states that the samples originated from the same distribution. The PE variation of the two different periods is statistically significant when the p-value is smaller than the significance level, which in this study we set it equal to 0.05 (5%). The advantages of this test are as follows: (a) the test does not make any assumptions about the population distribution that the samples were drawn from, and (b) even if the sizes n1 and n2 of the two samples are small, the test can still produce robust results as long as the quantity $N=(n1^{*}n2)/(n1+n2)$ is larger than 4. We applied the test in pairs of different periods (periods I and II, periods II and III) at each station during the three eruption cycles in January 2011, September–October 2017, and February–March 2018. The results of this test are summarized in Table 1

(See figure on next page.)

Fig. 2 Diagrams showing the variation of PE for station SMN during the three eruption cycles at Shinmoedake volcano. Spectrograms for the same time periods are shown at the bottom of each PE plot and spectral amplitudes follow the colored scales at the right. The double arrows on top of each diagram delineate the three different periods discussed in the main text. The green dashed line in the top panel indicates the time of the small phreatic eruption on 19 January 2011

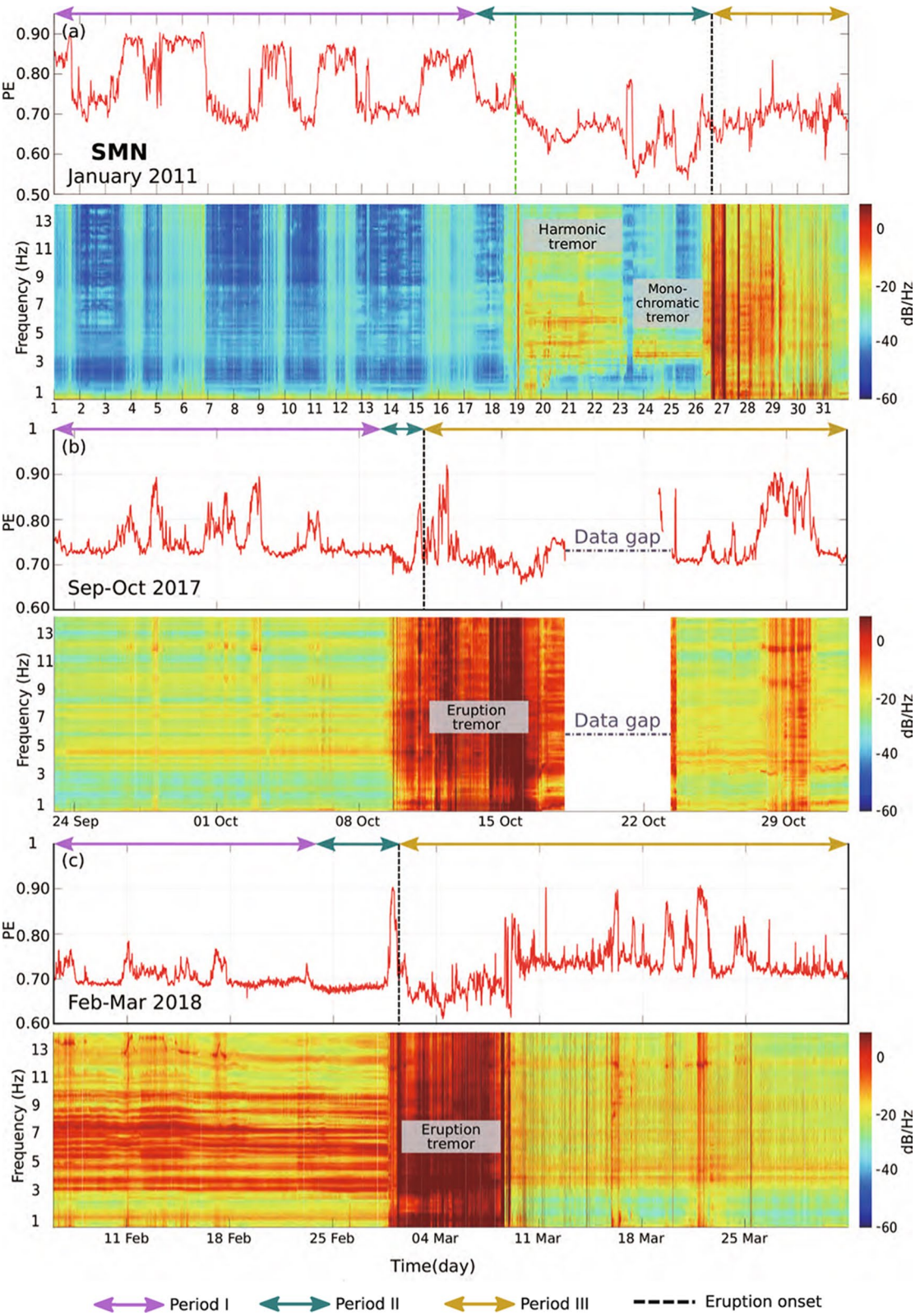

Fig. 2 (See legend on previous page.)

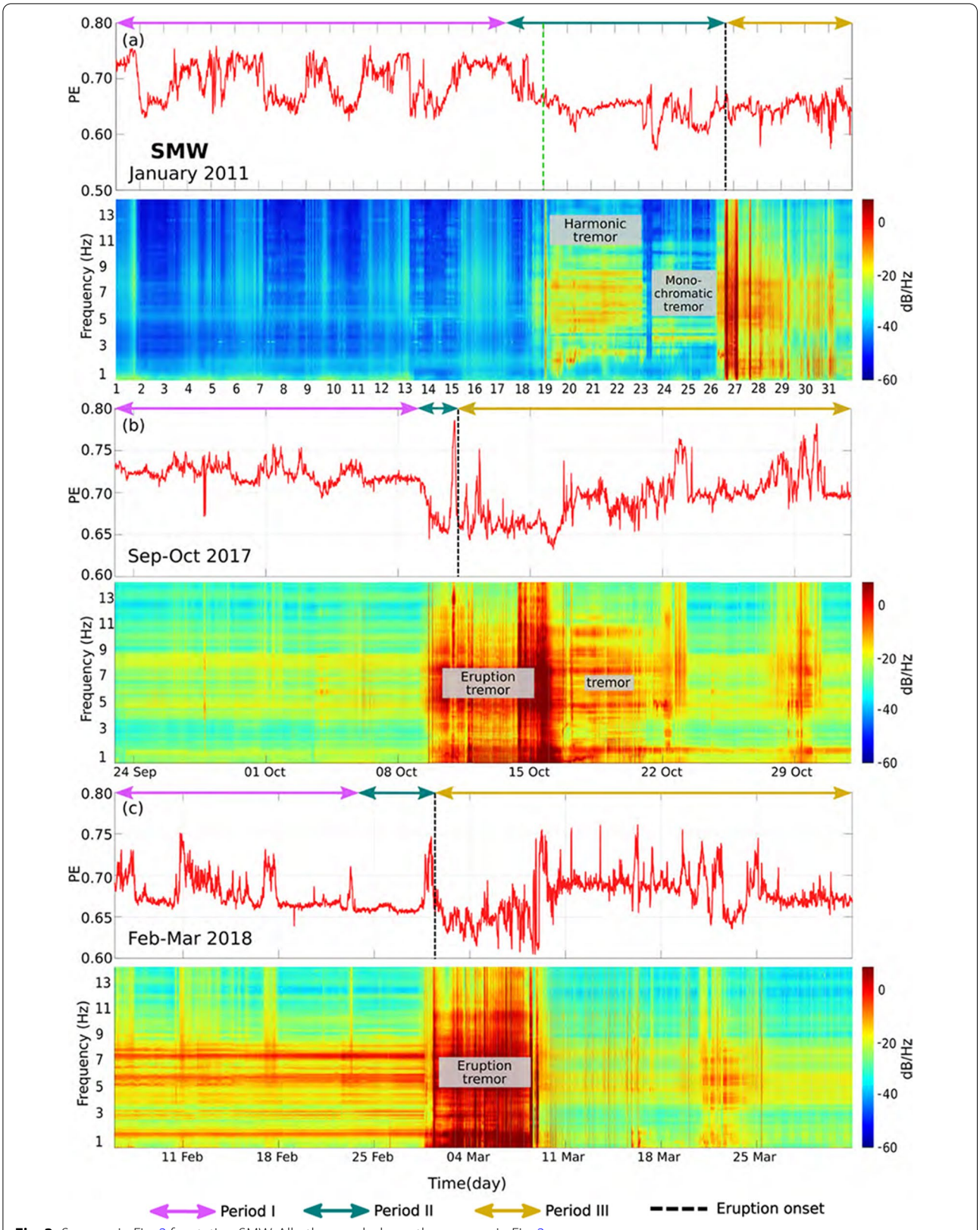

Fig. 3 Same as in Fig. 2 for station SMW. All other symbols are the same as in Fig. 2

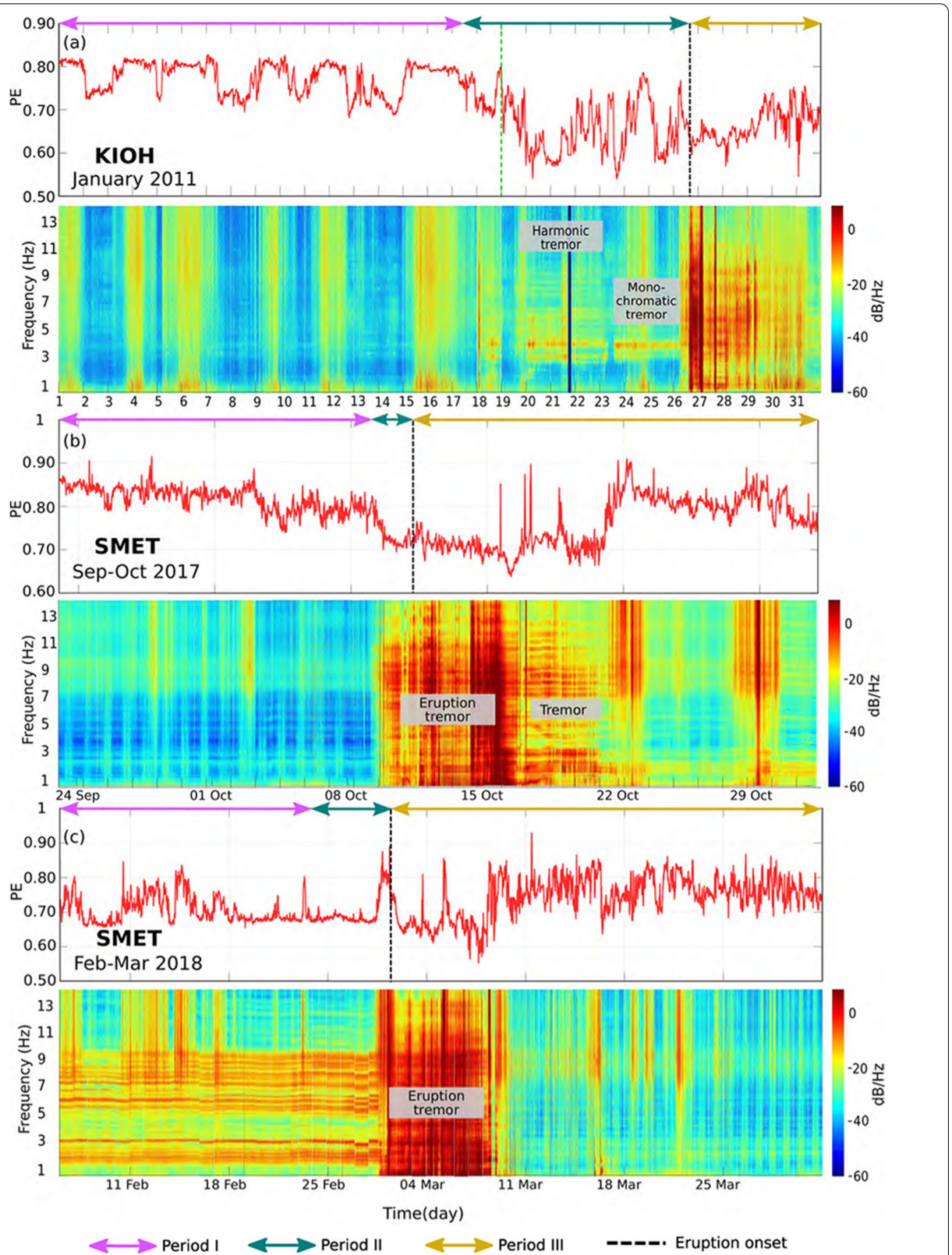

Fig. 4 Same as in Fig. 2 for station KIOH (active only during the 2011 eruption) and for station SMET (active during both 2017 and 2018 eruptions). All other symbols are the same as in Fig. 2

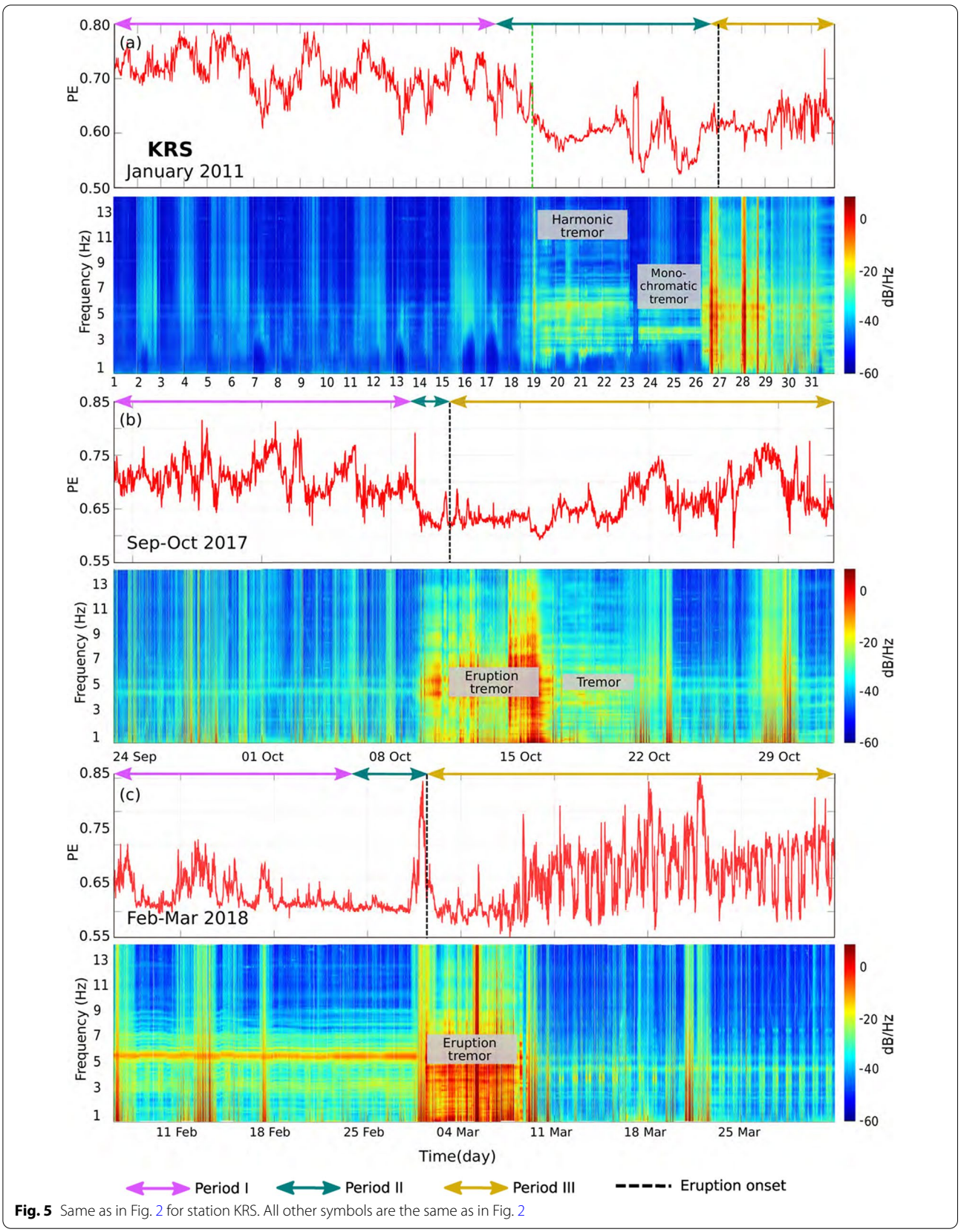

Fig. 5 Same as in Fig. 2 for station KRS. All other symbols are the same as in Fig. 2

Table 1 Summary of the results of the Kolmogorov–Smirnov test when applied to pairs of observation periods at all stations

Station	January 2011		October 2017		February–March 2018	
	I–II	II–III	I–II	II–III	I–II	II–III
SMN	$P<10^{-6}$	$P<10^{-6}$	$P<10^{-6}$	$P=0.12$	$P<10^{-6}$	$P<10^{-6}$
	$N=419.04$	$N=242.30$	$N=103.11$	$N=114.51$	$N=346.08$	$N=367.33$
SMW	$P<10^{-6}$	$P<10^{-6}$	$P<10^{-6}$	$P<10^{-6}$	$P<10^{-6}$	$P<10^{-6}$
	$N=419.04$	$N=242.30$	$N=103.11$	$N=114.51$	$N=346.08$	$N=367.33$
KIOH	$P<10^{-6}$	$P<10^{-6}$	–	–	–	–
	$N=419.04$	$N=242.30$				
SMET	–	–	$P<10^{-6}$	$P<10^{-6}$	$P<10^{-6}$	$P<10^{-6}$
			$N=103.11$	$N=114.51$	$N=346.08$	$N=367.33$
KRS	$P<10^{-6}$	$P<10^{-6}$	$P<10^{-6}$	$P<10^{-6}$	$P<10^{-6}$	$P<10^{-6}$
	$N=419.04$	$N=242.30$	$N=103.11$	$N=114.51$	$N=346.08$	$N=367.33$
TKS	$P<10^{-6}$	$P<10^{-6}$	$P<10^{-6}$	$P<10^{-6}$	$P<10^{-6}$	$P<10^{-6}$
	$N=419.04$	$N=242.30$	$N=103.11$	$N=114.51$	$N=346.08$	$N=367.33$

Each pair of periods contains the corresponding p-value and the metric N that should be larger than 4 in order for the test results to be reliable. Empty spaces denoted "–" for stations SMET and KIOH signify lack of data during January 2011 and October 2017, February–March 2018, respectively

and show that almost all p-values are less than 10^{-6} (almost zero) which is much lower than the significance level of 0.05, while N values are in all cases larger than 4. An exception to this pattern is the pair of periods II–III at station SMN during the October 2017 eruption cycle with a p-value (~ 0.12) that indicates similar PE distribution during these periods. Apart from this, we can conclude that the PE values between periods I–II and periods II–III are significantly different during the three eruption cycles at most of the stations.

Another question is what is the relationship between PE variation and the frequency of occurrence of volcano-tectonic earthquakes during the three eruption cycles. Additional file 1: Figs. S6–S8 in the supporting information also present histograms showing the distribution of earthquake occurrence at the same time scale as the PE variation at each station. We do not observe significant correlation between the two quantities despite the fact that isolated spikes in PE seem to coincide with increased number of earthquakes. This low degree of correlation is probably due to two factors: (a) small earthquakes have a duration in the order of a few to 10 s of seconds which is much smaller than the window length we used (20 min), and (b) such earthquakes exhibit significant energy at frequencies up to 15–20 Hz which are far higher than the corner frequency of 7 Hz we selected for filtering the data. As a result of these two factors PE is little influenced by the frequency of occurrence of volcano-tectonic earthquakes.

Discussion

PE variation during period I

The fluctuating PE values during 1–17 January 2011 were probably associated with weather disturbance, which was observed by the infrasonic microphone at station SMN. The infrasonic microphone recorded continuously the acoustic wave pressure in the atmosphere, including volcano explosions and wind noise. We observed that higher PE values coincided with higher amplitudes of the infrasound recording, while lower PE values coincided with lower amplitudes. The higher amplitudes of the infrasound recording were likely associated with wind activity around Shinmoedake volcano since these signals occurred periodically in a timescale of hours to days. Such a correlation between the infrasound recording and PE variation can be observed at SMN, SMW, and KIOH (Additional file 1: Fig. S10). We found that there was no clear relationship at KRS, probably due to increased noise levels, and at TKS due to its distance from the volcano. On the other hand, during period I in 2017 and 2018 the fluctuating PE pattern was less clear and there was no significant relationship among the PE variations and infrasound recordings (Additional file 1: Figs. S11, S12). The infrasound recordings at SMW and KRS2 stations exhibited little amplitude variation since they had a low signal-to-noise ratio. We also investigated the relationship of PE variation with precipitation recorded at Ebino weather station which is located 6 km to the NW of Shinmoedake (cf. Figure 1). During period I in 2017–2018 eruption cycles the precipitation levels were quite small and exhibited no correlation with PE variation (cf. Additional file 1: Fig. S11, S12). A careful look at the spectrograms shows that the fluctuating PE pattern in 2017 and 2018 likely coincided with the high frequencies that occurred periodically within each day. Hence, we infer that the fluctuating PE values during period I in 2017 and 2018 might be associated with anthropogenic noise.

PE variation during periods II and III

In January 2011, period II coincided with volcanic tremor that started 7 days before the subplinian eruption. The harmonic tremor occurred during 19–23 January, while the monochromatic tremor was recorded during 23–24 January. Volcanic tremor is probably generated by nonlinear source processes that exhibit deterministic behavior (Konstantinou 2002; Konstantinou et al. 2013) and this was also shown to be true for the case of Shinmoedake tremor (Natsume et al. 2019; Takeo 2021). The deterministic signal should correspond to lower PE values; hence, the occurrence and the spectral content of volcanic tremor were probably the factors that caused the decrease in PE values during period II in January 2011. Volcanic tremor at Shinmoedake during 2011 most likely had two sources, namely, a deeper one beneath the crater that was caused by magma flow (Matsumoto et al. 2013; Takeo 2021) as well as a shallower one that generated non-harmonic tremor and was associated with the shallow hydrothermal system beneath Shinmoedake (Nakamichi et al. 2013). The latter source was likely excited when high temperature magma migrated to shallower depth, transferring a significant amount of heat to the aquifer that resulted in the production of steam and bubbles. The bubbles then grew and collapsed continuously generating non-harmonic tremor within the aquifer. An aquifer layer was indeed imaged by use of magnetotelluric observations beneath the northern part of Shinmoedake, at depths between 1 km below sea level and 1 km above sea level (Kagiyama et al. 1996; Aizawa et al. 2014). In September–October 2017, period II occurred 2 days before the eruption. This coincided with the deformation change at the volcano edifice and LF events that occurred 38 h before the onset of the eruption (Yamada et al. 2019). The deformation involved a step-like change in tilt records at the closest tilt station to Shinmoedake (~3.1 km). The uplift deformation and LF events represented increasing fluid activity, such as magma intrusion or pressure buildup in the magma chamber (Yamada et al. 2019). The migration of high temperature magma or fluid to a shallower depth may result in higher attenuation of seismic waves. The attenuation mostly affects the high-frequency part of the seismic waves and thus results in a lower frequency signal that also corresponds to lower PE values.

The decreasing PE pattern before the 2018 eruption was less clear at all stations. The seismicity, tilt, and seismic velocity records also exhibited no significant precursory signals prior to the eruption and this was probably caused by the rapid ascent of magma (Yamada et al. 2019; Nishida et al. 2020; Matsumoto and Geshi 2021). Another possibility is that the decreasing pattern occurred several months prior to the 2018 eruption and the observation period of PE needs to be extended in order to identify such a decrease. Hence, we plotted the PE variation from April 2017 until May 2018 by calculating the lowest values every 3 days without overlap until the whole time series was analyzed (Fig. 6). The use of 3 days window length exhibited more obvious PE variation at all stations rather than 5 days or 7 days window length (Additional file 1: Fig. S13–S17). The extended PE observation showed a slight decrease in PE values, which was identified from early October 2017 until early March 2018 at SMN and SMW station, and from the middle of September 2017 until the beginning of March 2018 at station KRS. Meanwhile, such decreasing pattern was not observed at TKS station during the extended PE observation. This slight decrease coincides with the long-duration tremor episode that declined after the 2017 eruption and gradually increased again toward the 2018 eruption, according to JMA. However, firm conclusions about the long-term evolution of PE can be reached only after comparing PE with long-term geodetic, seismological, and meteorological data, which will be the focus of a future study.

An interesting feature was observed during period II when PE values exhibited a spike just before the onset of each eruption (cf. Figures 2, 3, 4 and 5). This feature was captured by almost all stations during the three eruption cycles, which implies that it is unlikely to be the result of local conditions around each station. These spikes may be related to bubble growth and collapse that was caused by the interaction between high temperature magma with the water contained in the shallow aquifer (Fig. 7a). When a thin water layer interacts with high temperature magma, the water would boil quickly generating bubbles rapidly and these bubbles will be collapsing in a random way. The bubble collapse likely generated high-frequency signals (e.g., Cannata et al. 2010) adding a stronger stochastic component that would correspond to higher PE values. We also suggest that a similar mechanism might have occurred just before the 2017 eruption (Fig. 7b). On the other hand, by 2018 the aquifer probably had shrunk considerably and the PE spike feature was likely generated by a different mechanism. Matsumoto and Geshi (2021) identified that the ash emission materials mainly consisted of particles from the hydrothermal and non-hydrothermal altered part of the 2011 solidified lava and from the material derived from the 2018 ascending magma head. Hence, the spike in PE values just before the 2018 eruption was probably associated with fracturing of the 2011 solidified magma as it was being pushed out of the conduit by fresh magma (Fig. 7c). Small fractures would therefore occur randomly very close in time just prior to the eruption and would generate stochastic seismic signals that result in higher PE values.

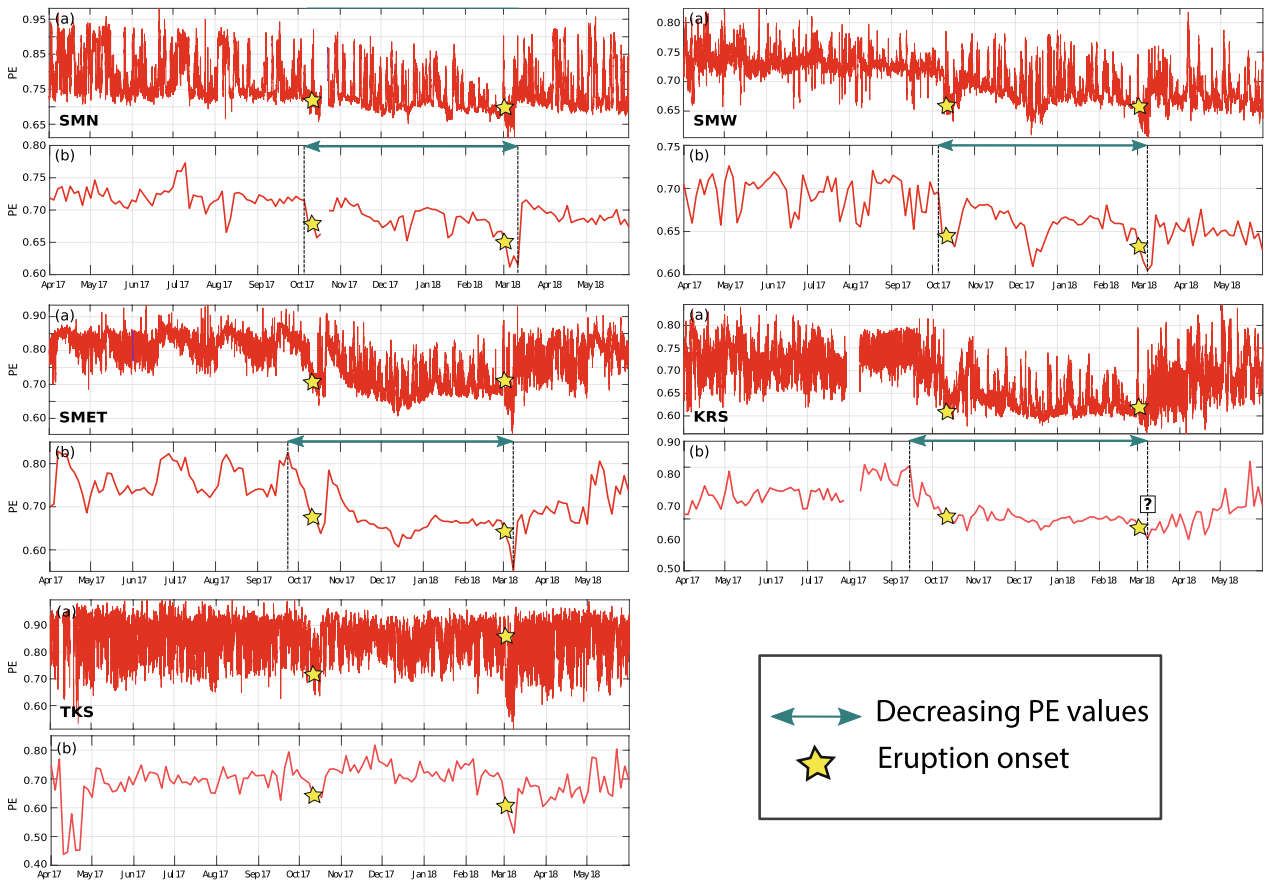

Fig. 6 Long-term variation of PE from April 2017 (shown as Apr17) until May 2018 (shown as May18) for stations SMN, SMW, SMET, KRS, and TKS. In each plot panel **a** shows the PE variation every 20 min, and panel **b** corresponds to the PE variation after applying a moving window of 3 days. At station KRS the end of the decreasing period of PE is not clear; hence, this is indicated by a question mark

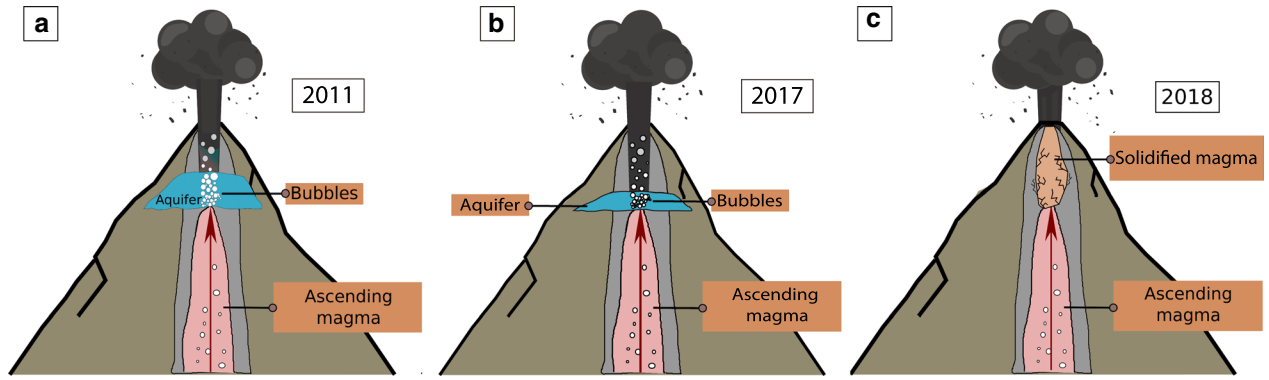

Fig. 7 Cartoon that summarizes the physical processes which took place in **a** 2011 when ascending magma interacts with the water of the aquifer, **b** 2017 when the aquifer has diminished in size, and **c** 2018 when the aquifer had evaporated and was replaced by solidified magma that was left over inside the conduit from previous eruptions (see text for details)

After the onset of the eruptions (period III), PE tended to have lower values for several days and then exhibited higher values subsequently during all three eruption cycles. Based on the spectral analysis, the lower PE values might be related either to eruption tremor or tremor occurring after the eruption (cf. Figures 2, 3, 4, and 5). In January 2011 volcanic tremor occurred 7 days before the eruption and continued until the end of that month. Volcanic tremor was also observed from 11 October 2017 until 21 October 2017, while in 2018 tremor was accompanied by ash emission and lava emplacement for 9 days. On the other hand, the higher PE values toward the end of period III were probably caused by the decreasing volcanic activity and increasing weather disturbances or anthropogenic noise around the volcano. This suggestion is supported by a comparison of PE variation and precipitation levels where increased rainfall generally coincides with the increase in PE values during period III (cf. Additional file 1: Fig. S11, S12).

Conclusions

In this work we evaluated the use of PE for monitoring seismic noise recorded by several stations at Shinmoedake volcano during three different eruption cycles. Results show that decreases of PE can be used in order to pinpoint periods of increased tremor activity and/or increased attenuation that usually precede explosive eruptions. The calculation of PE can be performed without much fine-tuning of parameters, since for practical applications both m and L can be assigned a limited number of values and any particular combination of these values does not affect the temporal variation significantly (cf. Additional file 1: Figs. S1–S5). These results support those of previous case studies (Glynn and Konstantinou 2016; Melchor et al. 2020; Konstantinou et al. 2022) and suggest that PE is potentially useful and can be easily incorporated into existing volcano monitoring schemes. The conclusions of this work are summarized as follows:

1. PE variations during the three eruption cycles were divided into 3 periods based on their general characteristics. Period I covered fluctuating PE values, period II was characterized by decreasing PE values, and the period after the onset of the eruption was defined as period III.
2. The fluctuating PE values (period I) might be related to weather changes in January 2011. However, PE fluctuations during period I in September–October 2017 and February–March 2018 were probably related to noise generated by human activities.
3. The decreasing PE pattern in period II was observed prior to all three eruption cycles, even though this was not as clear prior to the 2018 cycle. This decreasing pattern was likely associated with the occurrence of volcanic tremor and increased attenuation of the high-frequency seismic waves due to magma migration at shallower depth.
4. PE exhibited a spike-like increase and sudden decrease just before the eruptions in 2011, 2017, and 2018. In 2011–2017 this feature was probably associated with bubble growth and collapse due to the interaction between high temperature magma ascent and the aquifer. In 2018 the aquifer may have evaporated; hence, the spike in PE variation was likely related to the fracturing of solidified magma, which was being pushed out of the conduit by the 2018 magma.
5. During period III the PE variation was dominated by the occurrence of eruption tremor; thus, it attained relatively low values, however, as tremor activity ceased PE started increasing again as a result of local weather conditions and anthropogenic noise.

Supplementary Information

The online version contains supplementary material available at https://doi.org/10.1186/s40623-022-01729-9.

Additional file 1: Figure S1. Temporal variation of PE by using $m = 5$ (top) and $m = 6$ (bottom) with L=1,2,3,4,5,6 at station SMN. The variation of L is shown by different colors. The dashed line indicates eruption period in October 2017. **Figure S2.** Temporal variation of PE by using $m = 5$ (top) and $m = 6$ (bottom) with L=1,2,3,4,5,6 at station SMW. The other details of the figure are similar to Fig. S1. **Figure S3.** Temporal variation of PE by using $m = 5$ (top) and $m = 6$ (bottom) with L=1,2,3,4,5,6 at station SMET. The other details of the figure are similar to Fig. S1. **Figure S4.** Temporal variation of PE by using $m = 5$ (top) and m = 6 (bottom) with L=1,2,3,4,5,6 at station KRS. The other details of the figure are similar to Fig. S1. **Figure S5.** Temporal variation of PE by using $m = 5$ (top) and $m = 6$ (bottom) with L=1,2,3,4,5,6 at station TKS. The other details of the figure are similar to Fig. S1. **Figure S6.** PE variation per station for the period covering January 2011. The top panel shows a histogram of volcano-tectonic earthquakes per day according to the JMA catalog. **Figure S7**. The same as in the previous figure for the period September–October 2017. **Figure S8.** The same as in the previous figure for the period February–March 2018. **Figure S9.** The relationship between PE variation (red line) and spectrogram of vertical component waveforms recorded at TKS station in **a** January 2011, **b** October 2017, and **c** February–March 2018. **Figure S10.** Comparison between PE variation (red line) and infrasound recording (blue line) during 1–20 January 2011 at **a** SMN station, **b** SMW station, **c** KIOH station, **d** KRS station, and **e** TKS station. In January 2011, the infrasound microphone was set up only at station SMN. **Figure S11.** Comparison of PE variation (red line), infrasound recording (blue line), and precipitation data (purple bar) during October 2017 at station **a** SMN, **b** SMW, **c** SMET, **d** KRS, and **e** TKS. In October 2017, the infrasound recordings were observed at SMW and KRS2 stations, while the precipitation data were observed at Ebino weather station. **Figure S12.** Comparison of PE variation (red line), infrasound recording (blue line), and precipitation data (purple bar) during February–March 2018 at station **a** SMN, **b** SMW, **c** SMET, **d** KRS, and **e** TKS. **Figure S13.** PE variation from April 2017 until May 2018 at station SMN. **a** The PE variation (red line) in an extended period, **b** The lowest PE variation calculated using 3 days window length, **c** The lowest PE variation calculated using 5 days window length, **d** The lowest PE variation calculated using 7 days window length. **Figure S14.** PE variation from April 2017 until May 2018 at SMW station. **a** The PE variation (red line)

in an extended period, **b** The lowest PE variation calculated using 3 days window length, **c** The lowest PE variation calculated using 5 days window length, **d** The lowest PE variation calculated using 7 days window length. **Figure S15.** PE variation from April 2017 until May 2018 at SMET station. **a** The PE variation (red line) in an extended period, **b** The lowest PE variation calculated using 3 days window length, **c** The lowest PE variation calculated using 5 days window length, **d** The lowest PE variation calculated using 7 days window length. **Figure S16.** PE variation from April 2017 until May 2018 at KRS station. **a** The PE variation (red line) in an extended period, **b** The lowest PE variation calculated using 3 days window length, **c** The lowest PE variation calculated using 5 days window length, **d** The lowest PE variation calculated using 7 days window length. **Figure S17.** PE variation from April 2017 until May 2018 at TKS station. **a** The PE variation (red line) in an extended period, **b** The lowest PE variation calculated using 3 days window length, **c** The lowest PE variation calculated using 5 days window length, **d** The lowest PE variation calculated using 7 days window length.

Acknowledgements
The authors would like to thank T. Ohminato, M. Takeo, and A. Watanabe for their efforts to maintain the seismic stations in Kirishima. This collaborative work was made possible through the Sakura Science Exchange Program of the Japan Science and Technology (JST) and the visiting researcher program (for D.-A. Rahmalia program no P2020A0302180, I. Nurfitriana program no T2016T0322140) of the Earthquake Research Institute, University of Tokyo.

Author contributions
DAR and IN extracted the seismic data and performed all the necessary calculations under the supervision of KIK and MI. KIK and MI contributed in the study design and in the interpretation of the results. KIK wrote the manuscript, while all authors read the draft and approved the final version. All authors read and approved the final manuscript.

Funding
The first author would like to thank the Ministry of Science and Technology (MOST) of Taiwan for the financial support of this study through a grant. This study was also supported by the Ministry of Education, Culture, Sports, Science and Technology (MEXT) of Japan, under its Earthquake and Volcano Hazards Observation and Research Program.

Availability of data and materials
The seismic data belong to ERI, the University of Tokyo, and are not publicly available. However, all other materials included in this work (such as PE time series) can be obtained by the authors upon reasonable request.

Declarations

Competing interests
The authors declare that they have no competing interests.

Author details
[1]Department of Earth Sciences, National Central University, Jhongli 320, Taiwan. [2]Geophysical Engineering Program, Institut Teknologi Sumatera, South Lampung 35365, Indonesia. [3]Earthquake Research Institute, The University of Tokyo, Bunkyo-Ku, Tokyo 113-0032, Japan.

Received: 6 May 2022 Accepted: 27 October 2022
Published online: 30 November 2022

References

Aizawa K, Koyama T, Hase H, Uyeshima M, Kanda W, Utsugi M, Yoshimura R, Yamaya Y, Hashimoto T, Yamazaki K, Komatsu S, Watanabe A, Miyakawa K, Ogawa Y (2014) Three-dimensional resistivity structure and magma plumbing system of the Kirishima Volcanoes as inferred from broadband magnetotelluric data. J Geophys Res Solid Earth 119:198–215. https://doi.org/10.1002/2013JB010682

Amigó JM, Zambrano S, Sanjuán MAF (2008) Combinatorial detection of determinism in noisy time series. Europ Phys Lett. https://doi.org/10.1209/0295-5075/83/60005

Bandt C, Pompe B (2002) Permutation entropy: a natural complexity measure for time series. Phys Rev Lett 88:4. https://doi.org/10.1103/PhysRevLett.88.174102

Brenguier F, Shapiro NM, Campillo M, Ferrazzini V, Duputel Z, Coutant O, Nercessian A (2008) Towards forecasting volcanic eruptions using seismic noise. Nat Geosci 1:126–130. https://doi.org/10.1038/ngeo104

Cannata A, Di Grazia G, Montalto P, Ferrari F, Nunnari G, Patanè D, Privitera E (2010) New insights into banded tremor from the 2008–2009 Mount Etna eruption. J Geophys Res 115:B12318. https://doi.org/10.1029/2009JB007120

Cao Y, Tung WW, Gao JB, Protopopescu VA, Hively LM (2004) Detecting dynamical changes in time series using the permutation entropy. Phys Rev E 70:7. https://doi.org/10.1103/PhysRevE.70.046217

Geshi N, Takarada S, Tsuitsui M, Mori T, Kobayashi T (2010) Products of the August 22, 2018 eruption of Shinmoedake Volcano, Kirishima Volcanic Group, Japan. Bull Volcanol Soc Jpn 55:53–64

Glynn CC, Konstantinou KI (2016) Reduction of randomness in seismic noise as a short-term precursor to a volcanic eruption. Sci Rep 6:1–9. https://doi.org/10.1038/srep37733

Ichihara M, Matsumoto S (2017) Relative source locations of continuous tremor before and after the subplinian events at Shinmoe-dake in 2011. Geophys Res Lett. https://doi.org/10.1002/2017GL075293

Imura R (1992) Eruptive history of the Kirishima Volcano during the past 22 000 years. Geogr Rep Tokyo Metrop Univ 27:71–89

Kagiyama T (1994) Kirishima Volcanoes - Multi active volcanic group generated in a slightly tensile stress field. J Geog 103:479–487

Kagiyama T, Utada H, Yukutake T, Mogi T, Amita K (1996) Resistivity structure of the central and the southeastern part of Kirishima volcanoes. Bull Volcanol Soc Jpn 41(5):215–225

Kamata H, Kodama K (1999) Volcanic history and tectonics of the Southwest Japan Arc. Isl Arc 8:393–403. https://doi.org/10.1046/j.1440-1738.1999.00241.x

Kato K, Yamasato H (2013) The 2011 eruptive activity of Shinmoedake volcano, Kirishimayama, Kyushu, Japan-Overview of activity and Volcanic Alert Level of the Japan Meteorological Agency. Earth Planets Space 65:489–504. https://doi.org/10.5047/eps.2013.05.009

Konstantinou KI (2002) Deterministic non-linear source processes of volcanic tremor signals accompanying the 1996 Vatnajökull eruption, Central Iceland. Geophys J Int 148:663–675. https://doi.org/10.1046/j.1365-246X.2002.01608.x

Konstantinou KI, Perwira CA, Maryanto S, Surono A, Budianto MH (2013) Maximal Lyapunov exponent variations of volcanic tremor recorded during explosive and effusive activity at Mt Semeru volcano, Indonesia. Nonlin Processes Geophys 20:1137–1145. https://doi.org/10.5194/npg-20-1137-2013

Konstantinou KI, Rahmalia DA, Nurfitriana I, Ichihara M (2022) Fast Identification of volcanic tremor and lahar signals during the 2009 redoubt eruption using permutation entropy and supervised machine learning. Seism Res Lett 93(1):435–443. https://doi.org/10.1785/0220210176

Maeno F, Taniguchi H (2007) Spatiotemporal evolution of a marine caldera-forming eruption, generating a low-aspect ratio pyroclastic flow, 7.3 ka, Kikai caldera, Japan: Implication from near-vent eruptive deposits. J Volcanol Geotherm Res 167:212–238. https://doi.org/10.1016/j.jvolgeores.2007.05.003

Matsumoto K, Geshi N (2021) Shallow crystallization of eruptive magma inferred from volcanic ash microtextures: a case study of the 2018 eruption of Shinmoedake volcano, Japan. Bull Volcanol 83:1–14. https://doi.org/10.1007/s00445-021-01451-6

Matsumoto S, Shimizu H, Matsushima T, Uehira K, Yamashita Y, Nakamoto M, Miyazaki M, Chikura H (2013) Short-term spatial change in a volcanic tremor source during the 2011 Kirishima eruption. Earth Planets Space 65:323–329. https://doi.org/10.5047/eps.2012.09.002

Melchor I, Almendros J, Carniel R, Konstantinou KI, Hantusch M, Caselli A (2020) On data reduction methods for volcanic tremor characterization: the 2012 eruption of Copahue volcano, Southern Andes. Earth Planets Space 72:134. https://doi.org/10.1186/s40623-020-01270-7

Nakada S, Nagai M, Kaneko T, Suzuki Y, Maeno F (2013) The outline of the 2011 eruption at Shinmoe-dake (Kirishima), Japan. Earth Planets Space 65:475–488. https://doi.org/10.5047/eps.2013.03.016

Nakamichi H, Yamanaka Y, Terakawa T, Horikawa S, Okuda T, Yamazaki F (2013) Continuous long-term array analysis of seismic records observed during the 2011 Shinmoedake eruption activity of Kirishima volcano, southwest Japan. Earth Planets Space 65:551–562. https://doi.org/10.5047/eps.2013.03.002

Nakao S, Morita Y, Yakiwara H, Oikawa J, Ueda H, Takahashi H, Ohta Y, Matsushima T, Iguchi M (2013) Volume change of the magma reservoir relating to the 2011 Kirishima Shinmoe-dake eruption-Charging, discharging and recharging process inferred from GPS measurements. Earth Planets Space 65:505–515. https://doi.org/10.5047/eps.2013.05.017

Natsume Y, Ichihara M, Takeo M (2019) A non-linear time-series analysis of the harmonic tremor observed at Shinmoedake volcano, Japan. Geophys J Int 216:1768–1784. https://doi.org/10.1093/gji/ggy522

Nishida K, Mizutani Y, Ichihara M, Aoki Y (2020) Time-lapse monitoring of seismic velocity associated with 2011 Shinmoedake eruption using seismic interferometry: an extended Kalman filter approach. J Geophys Res Solid Earth. https://doi.org/10.1029/2020JB020180

Obermann A, Planès T, Larose E, Campillo M (2011) Imaging preeruptive and coeruptive structural and mechanical changes of a volcano with ambient seismic noise. J Geophys Res 118:6285–6294

Riedl M, Müller A, Wessel N (2013) Practical considerations of permutation entropy: a tutorial review. Eur Phys J Spec 222:249–262. https://doi.org/10.1140/epjst/e2013-01862-7

Staniek M, Lehnertz K (2007) Parameter selection for permutation entropy measurements. Int J Bifurc Chaos 17:3729–3733. https://doi.org/10.1142/S0218127407019652

Takeo M (2021) Harmonic tremor model during the 2011 Shinmoe-dake eruption Japan. Geophys J Int 224:2100–2120. https://doi.org/10.1093/gji/ggaa477

Yamada T, Ueda H, Mori T, Tanada T (2019) Tracing volcanic activity chronology from a multiparameter dataset at Shinmoedake Volcano (Kirishima), Japan. J Disaster Res 14:687–700. https://doi.org/10.20965/jdr.2019.p0687

Publisher's Note